

Supporting information

Table of contents:

1. Characterization of the illumination intensity
2. Power and polarization dependence of the measured photocurrent
3. AFM thickness characterization of the MoSe₂ crystals
4. Photocurrent spectra measurement process
5. Estimation of the gate-dependent Fermi energy

Characterization of the illumination intensity

The tunable laser source used for this work was a Solstis 2000 SRX-XF infrared Ti:Sapphire continuous wave laser from M-squared, with a wavelength range covering the spectral window between 700 and 1000 nm and a narrow linewidth of 1MHz. The Solstis infrared laser is driven by a Coherent Verdi 18W pump laser with a wavelength of 523nm. The output wavelength is registered using an Angstrom WS7 wavelength meter, connected to the Solstis laser by a single mode fiber. A power attenuation unit has been placed in the optical path to lower the output power of the laser from 3 W to around 15mW, to prevent damage to the sample.

To ensure a uniform distribution of the illumination intensity along our devices we telescope the laser beam using two lenses with different focal distances. Figure S1 shows the spatial distribution of the spot power density. The maximum value of the gradient of the power density is 50 mm^{-1} . The typical size of our devices is of $\sim 1 \mu\text{m}$. Consequently, even assuming the worst possible alignment between the sample and the laser spot, the power density can only change by 0.25% between the two electrodes.

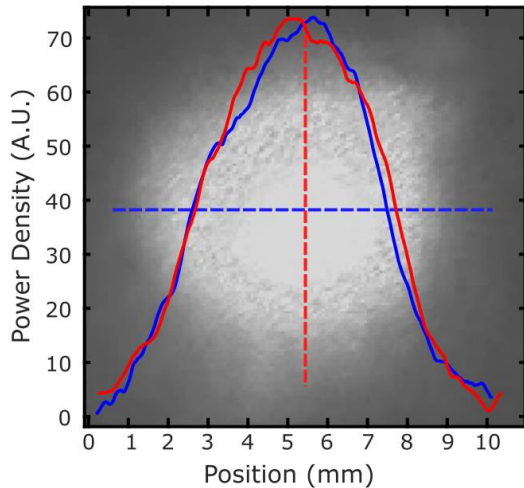


Fig. S1. Spatial distribution of the laser spot intensity along the horizontal (blue) and vertical (red) axis. The watermark below the plot is an optical image of the laser spot.

Power and polarization dependence of the measured photocurrent

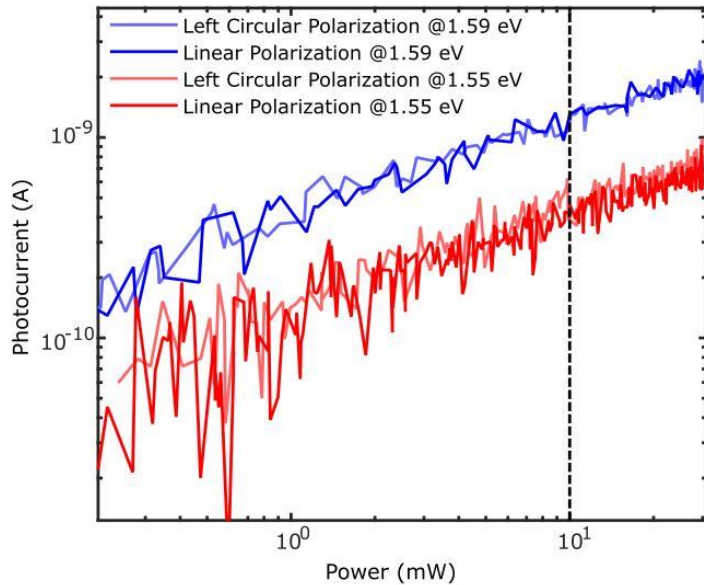


Fig. S2. Measured photocurrent for the monolayer device as a function of the laser power for two different polarizations (linear and left circular) and two different illumination energies: 1.59 eV (on resonance with the A⁰ excitonic transition) and 1.55 eV (off resonance).

Figure S2 shows a logarithmic plot of the measured photocurrent in the monolayer MoSe₂ phototransistor as a function of the illumination power, both for illumination on resonance with the A⁰ excitonic transition ($h\nu = 1.59$ eV) and off resonance ($h\nu = 1.55$ eV). We observe a sublinear dependence of the photocurrent, $I_{PC} \propto P^{0.48}$, for both illumination wavelengths, which indicates that both photoconduction and photogating play a role in the photocurrent generation [S1]. We do not observe any polarization dependence of the photocurrent, as expected when the illumination intensity is far enough below saturation.

MoSe₂ thickness characterization of the MoSe₂ crystals

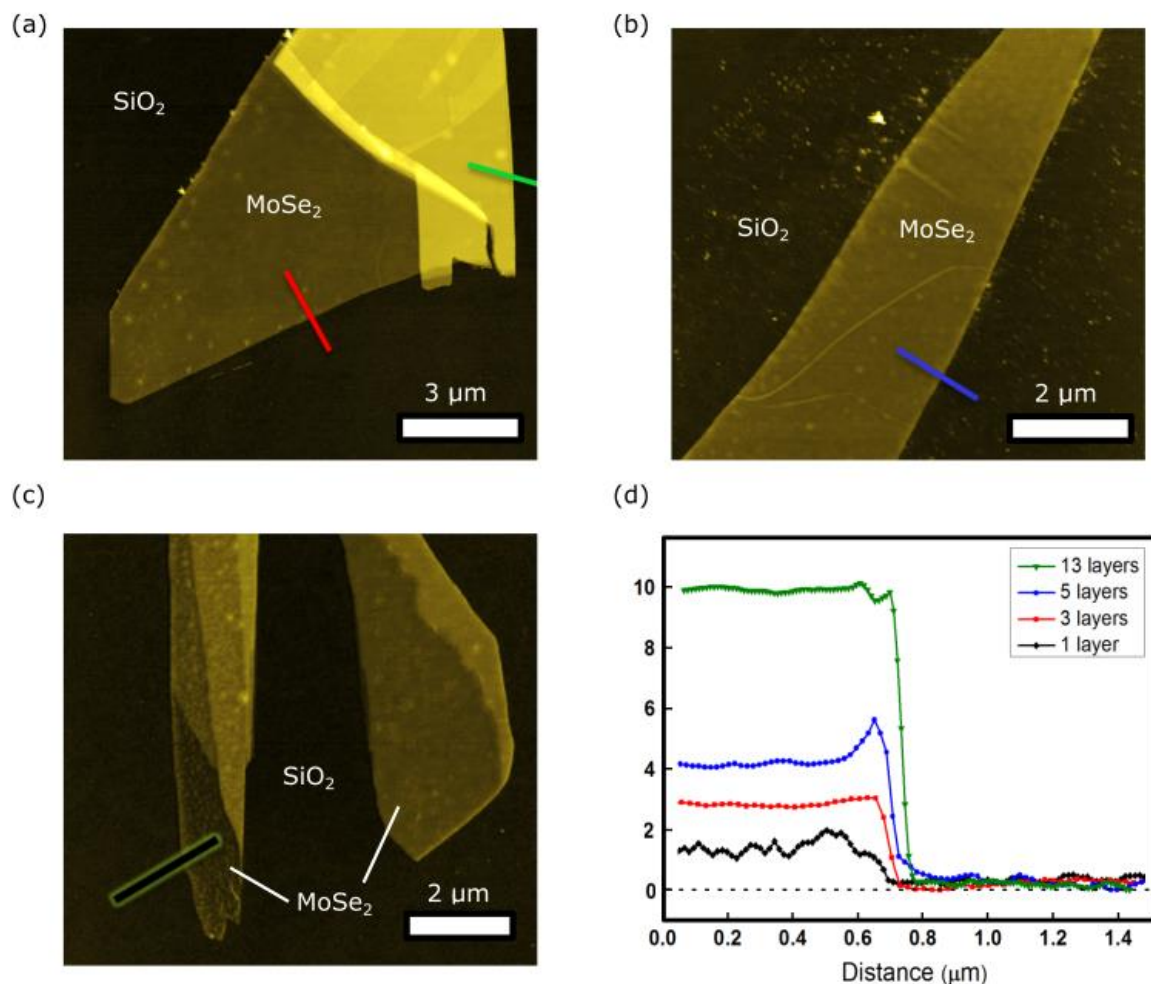


Fig. S3. (a-c) AFM topography images of the exfoliated MoSe₂ flakes on SiO₂ prior to the EBL processing of the electrodes. (d) Scan profiles along the lines marked in the AFM images.

Photocurrent spectra measurement process

To acquire a photocurrent spectral profile we start by applying a 5 V bias voltage between the electrodes of the device and then sweep illumination wavelength and measure the photocurrent through the following steps:

1. Set the laser at a specific wavelength
2. Measure the dark drain source current I_D
3. Open the shutter to illuminate the device
4. Wait for 0.1 s
5. Measure the bright drain-source current I_B
6. Close the shutter
7. Wait for 5 seconds

The photocurrent is then calculated as the difference between the measured bright and dark drain-source current $I_{PC} = I_B - I_D$. To improve the signal-to-noise ratio each measurement is repeated 20 times and the mean value is obtained.

Estimation of the gate-dependent Fermi energy

To estimate the variation of the Fermi energy induced by our gate voltage the Si/SiO₂/MoSe₂ stack can be modelled as a parallel plate capacitor, with a capacitance (per unit area) given by

$$C = \frac{\epsilon_r \epsilon_0}{d} . \quad (\text{S1})$$

where ϵ_r is the relative permittivity of SiO₂, ϵ_0 is the permittivity of vacuum, and d is the thickness of the SiO₂ layer. The areal density n of conduction-band electrons in the MoSe₂ crystal can then be estimated using

$$n = \frac{C}{e} (V_g - V_0) , \quad (\text{S2})$$

where e is the electron charge, V_g is the gate voltage and V_0 is an offset voltage that accounts for the fact that the conduction band only starts to be filled when the Fermi energy is close to the conduction band. The calculation of V_0 will be discussed below.

The carrier density, n , must also be equal to the total number of occupied states $\mathcal{Q}(E_F)$ in the conduction band:

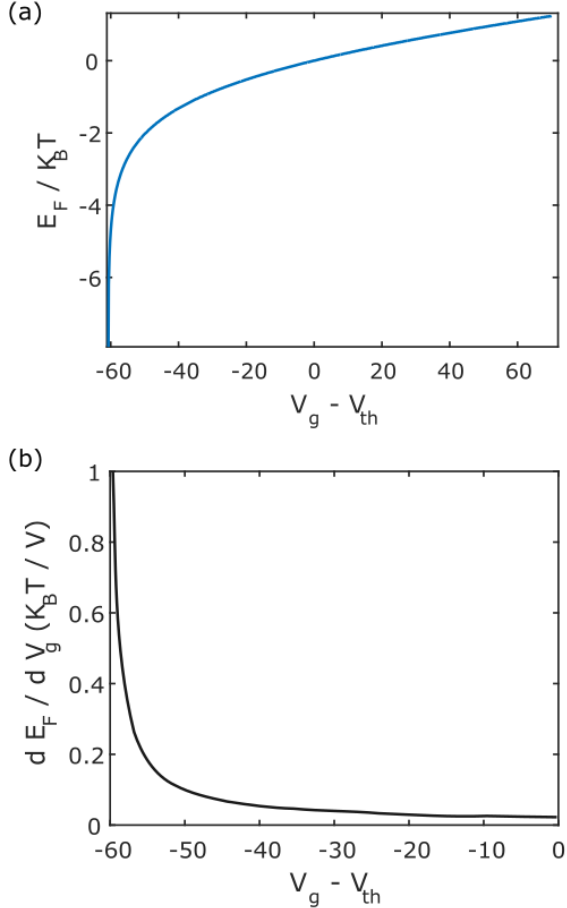


Fig. S4. (a) Calculated gate-dependent Fermi energy of the MoSe₂ crystal, in units of the thermal energy k_BT . (b) Numeric derivative of the Fermi energy as a function of the gate voltage.

$$\Omega(E_F) = \int_{-\infty}^{\infty} f(E, E_F) \times g_{2D}(E_F) dE = n \quad (\text{S3})$$

where $f(E, E_F)$ is the Fermi-Dirac distribution at room temperature and $g_{2D}(E_F)$ is the density of states of a two-dimensional free electron Fermi gas, given by

$$g_{2D}(E_F) = \begin{cases} \frac{m_e^*}{2\pi\hbar^2} g_s g_v & \text{if } E \geq 0 \\ 0 & \text{if } E < 0 \end{cases} \quad (\text{S4})$$

where m_e^* is the effective electron mass at the conduction band, $m_e^* = 0.6 m_e$, $g_s = 1$ is the spin degeneracy and $g_v = 2$ is the valley degeneracy. The energy $E = 0$ is chosen to be at the bottom of the conduction band.

Then, equation S3 yields

$$n = \frac{m_e^*}{\pi \hbar^2} \int_0^\infty f(E, E_F) dE . \quad (\text{S5})$$

Replacing n by its value from equation S1b and reordering terms we get

$$\int_0^\infty f(E, E_F) dE = \frac{C}{e} \times \frac{\pi \hbar^2}{m_e^*} (V_g - V_0) . \quad (\text{S6})$$

Finally, we derive the value of V_0 from a measured value of the threshold voltage, V_{th} , which is the voltage at which the Fermi energy is exactly at the bottom of the conduction band: $E_F(V_{\text{th}}) = 0$. From the transfer characteristics of the monolayer device we estimate a value of $V_{\text{th}} \sim 30$ V (using how the linear behavior at high V_g extrapolates to zero current). Then,

$$\int_0^\infty f(E, 0) dE_F = \frac{C}{e} \times \frac{\pi \hbar^2}{m_e^*} (V_{\text{th}} - V_0) , \quad (\text{S7a})$$

$$\Rightarrow V_0 = V_{\text{th}} - \frac{e m_e^*}{C \pi \hbar^2} \int_0^\infty f(E, 0) dE . \quad (\text{S7b})$$

Note that, at zero temperature, $f(E, 0)$ is a step function and the integral in equation S6b is zero.

Replacing V_0 in equation S5 we finally get

$$\int_0^\infty f(E, E_F) dE = \frac{C}{e} \times \frac{\pi \hbar^2}{m_e^*} (V_g - V_{\text{th}}) + \int_0^\infty f(E, 0) dE . \quad (\text{S8})$$

This equation must be solved numerically to obtain $E_F(V_g)$.

Fig. S4a shows the calculated Fermi energy as a function of the gate voltage, and Fig. S4b shows the numerical derivative of the Fermi energy, dE_F/dV_g . As observed, at the threshold voltage V_{th} the variation of the Fermi energy with the gate voltage is negligible compared with the thermal energy, $k_B T = 25$ meV. However, when the gate voltage is around 50 V below the threshold voltage, i.e. when the Fermi energy is $E_F \sim -2 k_B T$, the conduction band is only populated by thermally excited electrons, and a much higher increase in the Fermi energy is required to increase the number of charge carriers by the same amount. In consequence, in this voltage range, the variation of the Fermi energy with the gate voltage is comparable with $k_B T$.

References

- [S1] M. M. Furchi, D. K. Polyushkin, A. Pospischil, T. Mueller, *Nano Lett.* **2014**, 22.